Measuring the Effective Young's Modulus of Structural Silicone Sealant in Moment-Resisting Glazing Joints

Adam D. Lee[a,b,*], Paul Shepherd[a], Mark C. Evernden[a], David Metcalfe[c]

[a] *Department of Architecture and Civil Engineering, University of Bath, Claverton Down, Bath, BA2 7AY, U.K.*
[b] *PTCC Facade Design, Telecom Plaza, 316 Senator Gil Puyat Ave., Makati City, Metro Manila, 1200, Philippines.*
[c] *Centre for Window and Cladding Technology (CWCT), The Studio, Entry Hill, Bath, BA2 5LY, U.K.*

Abstract

Structural silicone sealants are synthetic rubber adhesives used in the construction industry to bond glass and other sheet infill materials to the frames of windows and curtain walls. In this paper, two different algebraic expressions are proposed to describe the way in which the rotational stiffness of the adhesive connection – resistance to moments acting about the axis of the joint – varies with the sealant's cross-sectional dimensions and elastic modulus. Laboratory testing of DC-983, a two-component structural silicone sealant used widely in factory prefabricated glazing applications, has, with some caveats, validated the mathematical models.

Keywords: facade design, structural silicone sealant, structural glazing, elastic modulus, curtain wall, mullion,

1. Introduction

In the middle of last century there began to emerge, hand in hand with the glass box architectural style, a new method of constructing tall buildings. First, a frame made up of columns and beams was erected, to support the

*Corresponding Author
Email addresses: adamlee@torstencalvi.com (Adam D. Lee), p.shepherd@bath.ac.uk (Paul Shepherd), m.evernden@bath.ac.uk (Mark C. Evernden), david.metcalfe@cwct.co.uk (David Metcalfe)

http://dx.doi.org/10.1016/j.conbuildmat.2018.06.038

floors; then, to keep out the weather, the freestanding structure was enclosed with a lightweight, metal framed, skin [1, 2, 3]. Since that time, designers of these exterior "curtain walls" have been using the same set of assumptions when modelling the forces that are transferred from the sheet material covering the facade, which is often glass, to the members in the supporting frame. These structural idealizations are illustrated in Figure 1, in four cross-sections through extruded aluminium "mullion" profiles, which are those that span vertically from one floor to another.

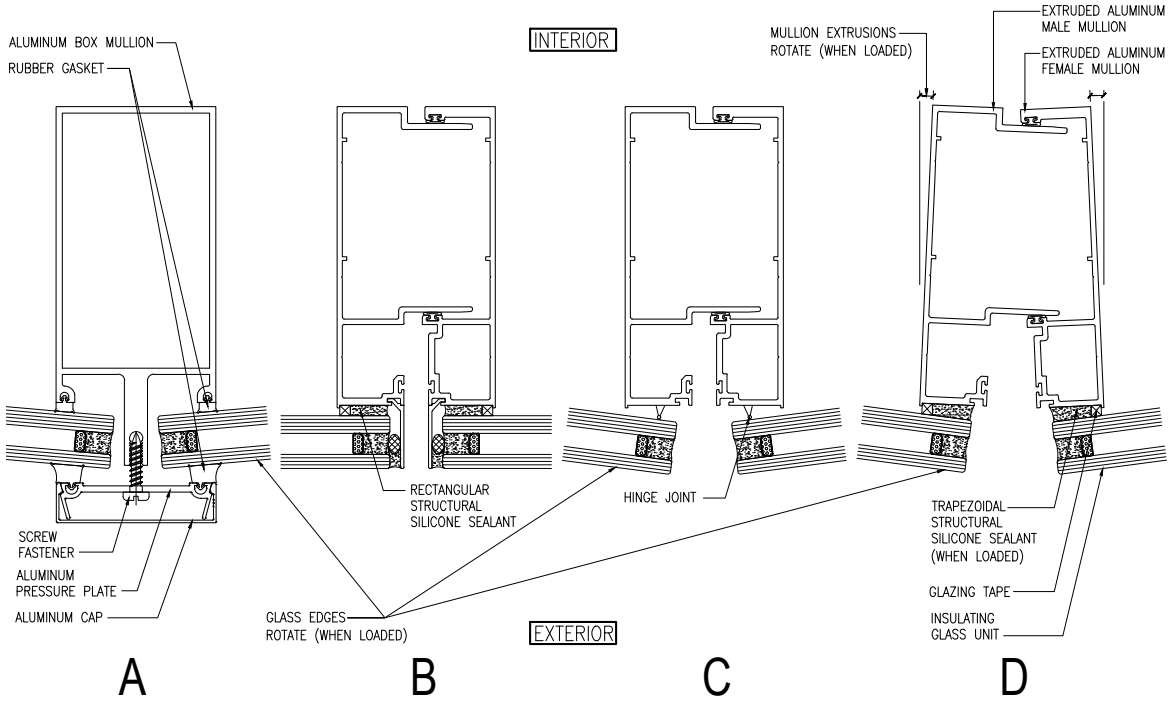

Figure 1: Cross-sectional shapes of vertical mullions. In detail "A", glass is held mechanically to a simple box section. Structural sealant, in detail "B", bonds glass to the male and female profiles of a unitized wall's split mullion: this design's structural idealization is shown in "C", although "D" may be a better represent the wall's actual behaviour when subjected to wind load.

The first of the mullions, Figure 1-A, is a simple box section. Aluminium curtain wall profiles of this sort, which must be cut and assembled at the construction site, became popular in the 1960s [e.g. 2] and, for some applications,

are still in use today. Glass is retained at the face of the wall system using a mechanical clamp. Rubber gaskets permit relative movement, in the plane of the wall, between the glass and the metal frame. So, the glass does not prevent the aluminium members from moving laterally. Also, the mechanical clamp at the edge of the glass permits rotation, as shown in Figure 1-A, so glass deflections do not cause the framing member to twist about its longitudinal axis.

Another means of securing glass to its frame is to use an adhesive. This approach, known as "structural glazing" and shown in Figure 1-B, is relatively new. The first high-rise tower with a structurally glazed curtain wall was completed as recently as 1986 [4, p. 53]. Since then, architects have embraced the new aesthetic, using the technology to create large, flat facades, without any metal components to the exterior of the glass. Structural glazing has become a common and conspicuous feature of large buildings around the world. Current structural design methods and usage guidelines for the adhesives – structural silicone sealants – are detailed in ASTM C1401 [5]. The reasons for inclusion of the "glazing tape" shown in Figures 1-B and 1-D, and the effect that this tape has upon structural performance, are explained in Section 7.3.

Figure 1-B shows the E-shaped male and female extrusions that together form the split mullion of a modern unitized curtain wall. In such designs, the facade is made up of discrete panels that can be prefabricated. Because of this, and other, practical advantages [6 p. 4-5; 7 p. 86], the great majority of the world's new curtain wall is of this type [8, p. 82]. From a structural standpoint however, the split mullion's narrow profiles are, in torsion, less rigid than the box sections they replace (Figure 1-A). Consequently, it is frequently the case that prevention of buckling is the dominant concern for today's facade engineers.

Lateral torsional buckling (LTB) is the mode of structural failure caused and characterized by extreme axial rotation of a flexural member's cross section. At the onset of failure by LTB, a glazing system's profiles deflect in the manner shown in part D of Figure 1. The analysis of LTB is complex [e.g. 9, Chapter 5], and is affected by parameters aside from bending moment distribution, material properties, cross-sectional shape and distance between supports. Other

significant particulars are the member's initial straightness, and also the load eccentricities, which may themselves be functions of the profile's rotation.

If one of a member's flanges is restrained to prevent it from rotating about its long axis, then LTB can be prevented. The moments that are transferred to such braces can be estimated analytically [e.g. 9, Equation 12.10], and the magnitude of the required torsional resistance is small. In a typical, unitized curtain wall system, the panes of glass or other sheet infill materials that are connected to the mullion's outer flanges have ample structural capacity to serve a torsional braces. However, current design guides advise that, even in structurally glazed systems, glass and infill materials should not be considered to be restraints [e.g. 10]. Consequently, in structural analysis, mullions are modelled [as in 11, Part VIII, pp. 56-61] with the assumption that no moment is imparted to them by the glass. The structural idealization of the glass support is a hinge, as shown in Figure 1-C.

In reality, because the structural sealant joint has stiffness, Figure 1-D might better describe a unitized mullion's mid-span condition under wind load. In this diagram, positive wind pressure causes the glass to deflect toward the interior of the building and, as a consequence, moment is transferred through the structural silicone sealant to the mullion profiles, whose inner flanges move toward each other. The onset of LTB in the mullion profiles will, therefore, be affected by the moment resistance of the sealant joint.

Facade engineers are interested in improving current methods of predicting LTB [12, 13] because, with continuing advances in the sizes of the panes that can be processed by glass fabricators, the structural members in exterior wall systems are becoming increasingly slender [10]. Research by others [e.g. 14] suggests that a structural silicone joint may provide sufficient support to prevent LTB in some cases, but a recent survey [12] showed that facade design professionals have insufficient information to assess whether an attachment to a glazing system's frame will be effective as an LTB restraint. The analytical steps proposed in this present paper might therefore be incorporated in a more comprehensive model, to predict the angle through which a framing extrusion will

rotate when full design load is applied, and thus demonstrate that the frame's resistance to LTB is adequate.

Intuitively, it might seem dangerous to create structures using metal flexural members that remain stable only because they are supported by restraints made of glass. Glass is, after all, a brittle material, and building facades must be designed with the expectation that occasional breakages will occur. It is therefore worth explaining that the governing design loads acting upon a building's facade are usually wind pressures. So, if breakage destroys a pane, it is true that its frame will no longer be restrained by the glass but, at the same time, the frame will no longer receive wind load. Therefore, failure of the glass will not cause a failure of the metal structure that it restrains.

With greater understanding of the joint's behaviour and with a more sophisticated structural model, it may be possible to reduce the mass of metal required to construct a curtain wall. The opportunity for metal savings exists because, in the design of modern mullion extrusion shapes, it is common that stability – in particular, resistance to lateral torsional buckling – is the governing structural design consideration. If structural sealant joints can be shown to provide effective lateral or torsional restraint for their frames, then facade engineers will be able to make use of lighter profiles [e.g. 14]. The pursuit of efficient curtain wall design solutions is worthwhile, not only because of the cost savings that can be attained by reducing material usage, but also because, amongst common building materials, the embodied energy in aluminium is unusually high [15, p. 74] and so significant environmental benefit can be achieved by controlling metal content [16].

The manner in which a mullion profile might be caused to rotate about its lengthwise axis is illustrated in Figure 1-D. When the magnitude of this rotation is sufficiently large then, aside from any structural consequences, other functions of the wall can be affected. For example, it is possible that the interior flanges of the male and female profiles will disengage, breaching the weather seal. Curtain wall system failures of this sort, caused by excessive rotation of a member about its extrusion axis, could be predicted during the design process

if facade engineers were provided with a model of the relationship between moment and rotation in a structural silicone joint. For these two reasons – firstly to help curtain wall designers determine whether a particular structural sealant connection can provide torsional bracing for a mullion, and secondly to quantify the axial moment transmitted – the objective of the research described in this paper has been to develop a simple algebraic method to describe the rotational stiffness of a structural sealant joint, and to collect experimental data with which to validate the mathematical model.

The terms "elastic modulus", "Young's modulus" and "modulus of elasticity" are equivalent, and may be used interchangeably. For a sealant, the published value of this property is usually that measured 14 days [e.g. 17] or 21 days [18] after creation of the sample. Research [17, p. 967] has, however, revealed that the Young's modulus of a particular structural silicone sealant, DC-995, can rise dramatically during the 100 days following the assessment on day 14. In that single-component sealant – one that does not need to be mixed with a separate catalyst prior to application – the increase in elastic modulus "was in the range of 850-950 %". If the results of this study are to be applied in practice then there is a need to understand the changes in Young's modulus that occur as a sealant ages. Therefore, the rotational stiffness of a two-component sealant, DC-983 – a type that is commonly used when structurally glazed curtain wall panels are prefabricated in a factory – has been assessed at 14, 114 and 214 days. Also, each sample's indentation hardness was measured at 214 days.

Apart from the rubber pads used in vibration-absorbing mountings, elastomeric materials are rarely encountered in building structures, and it may therefore be helpful to summarize their special properties. Structural silicone sealants are viscoelastic, meaning that an applied load causes damped elastic deflection, and so the magnitude of stress depends not just upon the magnitude of strain, but also upon the rate of change in strain. Figure 2, shows the relationship between tensile stress and strain [19, Table 1] for the particular sealant that has been tested in this study, DC-983. It can be seen that, even when strain is increased at a constant rate, in accordance with ASTM C1135 [18],

the material's behaviour is not linear-elastic. If, however, the product is used within the allowable range defined by the manufacturer, so that strain does not exceed 25 %, then a linear-elastic idealization results in a maximum error of less than 9 %.

While considering the precision with which a sealant's elasticity can be modelled, it should be noted that the expected level of variability in laboratory measurements is high. If a sealant's stress is measured twice, at 10 % tensile strain, using the ASTM C1135 method, there is 95 % probability that the two measurements will differ by less than 0.041 MPa (6 lbf/in^2) if the tests are carried out in the same laboratory, or by 0.090 MPa (13 lbf/in^2) if carried out in different laboratories [18, Table 1]. For the DC-983 sealant tested in this present study, these 95 % probability ranges are, respectively, equivalent to 20.7 % and 44.8 % of the published value of stress at 10 % strain, which is 0.2 MPa [20].

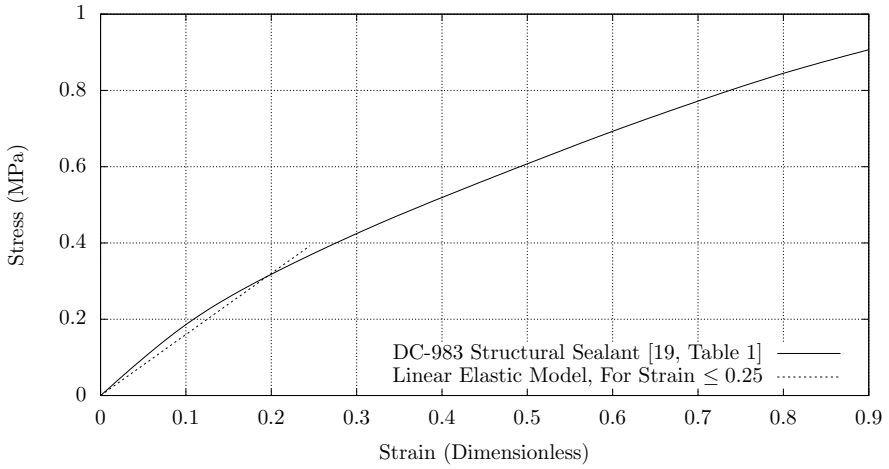

Figure 2: Stress with respect to strain in DC-983 structural sealant, measured by the ASTM C1135 laboratory method [18]. Also plotted is a linear idealization, for the useable range defined by the sealant manufacturer, in which strain is limited to 25 %.

2. Algebraic Model of Moment Resistance

In the model that is commonly used by practising facade engineers to assess the load capacity of a structural sealant joint [5, Section 30], it is assumed

that the glass remains flat when wind pressure is applied, and that the sealant experiences only tensile or only compressive stress. Several researchers [e.g. 21] have carried out sealant analyses that take glass deflection and the sealant's shear stresses into account. In these more sophisticated studies, solutions for particular design conditions have been obtained numerically, using finite difference or finite element techniques. While the results obtained in this way are comprehensive – the entire stress field is revealed – the process of preparing numerical models is time consuming, making it impractical to use this approach to investigate the many and varied design cases that might be encountered in a real building's facade. It has therefore been this present study's aim to find, and to validate experimentally, a set of simple, closed-form algebraic expressions that may, in the future, be incorporated in a design code.

For the sake of simplicity, here the assumption will be made that structural sealants obey Hooke's law. The validity of this approach is discussed later, in Section 7.1. Adopting a linear-elastic model makes it possible to consider separately the different components of load, and to sum their effects using superposition. The application of a pure moment causes a unit length of sealant joint to deform elastically from its original rectangular cross section into a trapezoid, as shown in Figure 3, then the force in the equivalent couple, F, can be expressed in terms of the sealant's Young's modulus, E_{ss}. Considering either side of the sealant joint – the area in compression or the area in tension – the mean stress is half of the extreme fiber stress. Also, recalling that the force required to extend a linear-elastic material is the product of cross sectional area, strain and elastic modulus:

$$F = \frac{B\Delta g E_{ss}}{4g}\,, \tag{1}$$

where B is the "bite" or width of the adhesive plane, g is the "glueline" or sealant thickness, and Δg is the maximum distance through which the sealant extends. Similarly, the sum total moment per unit length of sealant joint, M, can be obtained by integrating torque over the width of the triangular compression

and tension zones that have been shaded in Figure 3:

$$M = \frac{2E_{ss}}{g} \int_{x=0}^{\frac{B}{2}} \frac{2x^2 \Delta g}{B}\, dx, \tag{2}$$

if the x-axis is horizontal in the right hand diagram of Figure 3. Hence:

$$M = \frac{B^2 \Delta g E_{ss}}{6g}. \tag{3}$$

If the eccentricity of F from the joint's centreline is Q then $M = 2FQ$. Substituting for F and M from Equations 1 and 3 gives the value of Q, which is $B/3$. This is, plainly, the standard result for a triangular load zone, in which the amplitude of force varies linearly with distance.

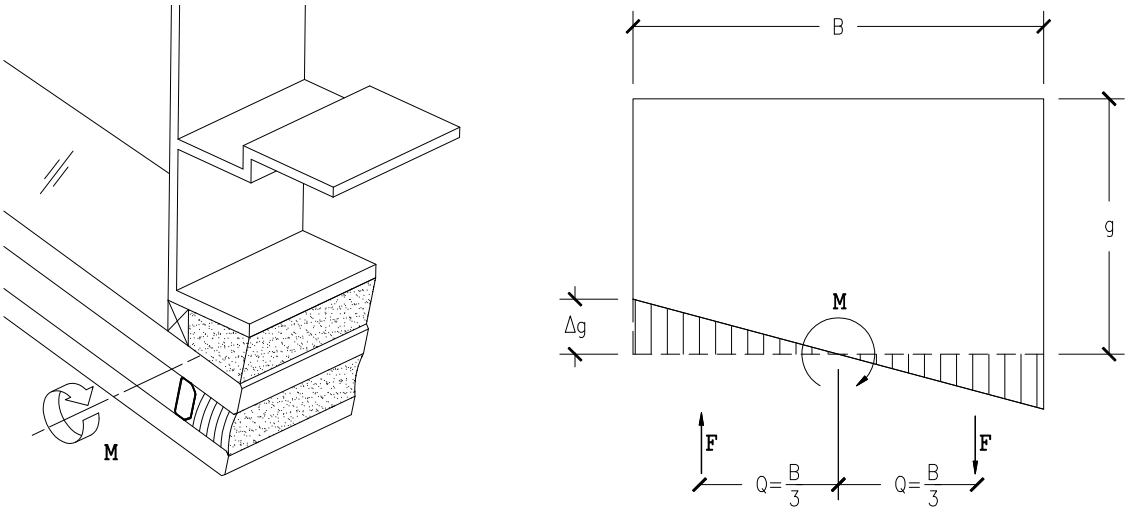

Figure 3: The edges of a glass pane rotate *(Left)* under the action of wind pressure. A section through the loaded structural sealant joint *(Right)* shows its trapezoidal shape.

If the angle through which the glass edge rotates is α then, from Figure 3, $\tan\alpha = 2\Delta g/B$. These rotations are small – usually only a few degrees – and so α is a close approximation to $\tan\alpha$, when α is measured in radians. This small angle assumption is reasonable while α is less than 0.176 radians (10 degrees).

In this range, $\alpha = 2\Delta g/B$, and Equation 3 can be rewritten:

$$M = \alpha \frac{B^3 E_{ss}}{12g}. \tag{4}$$

3. A More Sophisticated Model of Moment Resistance

Wolf and Cleland-Host [22] used a polynomial expressions to describe relationship between stress and strain in two-part structural silicone sealants. Their coefficients, below, were chosen to fit the experimentally determined responses of two commercial products, A and B, that had been tested at 22°C after one year of aging. For a given strain, ε, the corresponding stress, f, was found to be:

$$f_A(\varepsilon) = 0.87244\varepsilon^5 - 1.74222\varepsilon^4 + 1.59336\varepsilon^3 - 1.17958\varepsilon^2 + 1.01308\varepsilon \tag{5}$$

$$f_B(\varepsilon) = 3.80874\varepsilon^5 - 7.37014\varepsilon^4 + 4.44015\varepsilon^3 - 1.02037\varepsilon^2 + 0.93614\varepsilon \tag{6}$$

These two stress-strain curves are plotted in Figure 4.

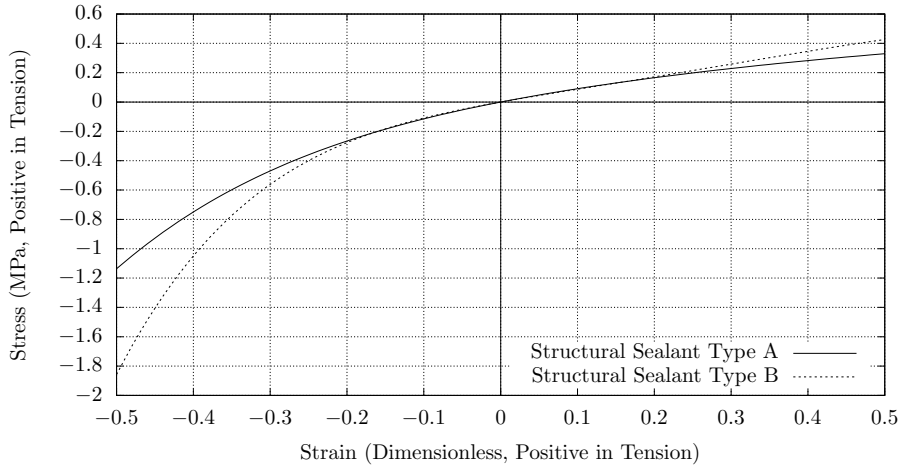

Figure 4: Curves chosen by Wolf and Cleland-Host [22, Table 2] to fit experimental measurements of stress and strain in two different two-part structural silicone sealants.

The market names of the sealant products tested by Wolf and Cleland-Host were not revealed, and so it cannot be assumed that their elastic properties

will match those of the sealant tested in this study, or those of the sealant used in a given glazing system. However, in Figure 4 it can be seen that the sealants' elastic moduli are greater in compression than they are in tension, and in this discussion the presumption is that such asymmetry is typical amongst all structural silicone sealants. A further supposition is that the stress-strain curve for any particular structural glazing sealant, or a reasonable approximation to it, can be obtained by applying a constant scaling factor to the stress function in Equation 5 or 6. Expressed another way, for a sealant Z:

$$f_Z(\varepsilon) \simeq k_Z f_A(\varepsilon), \tag{7}$$

where k_Z is a constant.

While formulating the previous rotational stiffness model, described in Section 2, the stress-strain curve from a tensile test was examined, and it was argued that, within the range between zero and 25 % strain, a linear-elastic approximation is sufficiently accurate for engineering design purposes. A constant value of Young's modulus was then assumed to apply in the sealant joint's tension zone, and also in the compression zone. Because of its simplicity, that previous model still may be of interest to engineers, but, in reality, Young's modulus is a function of strain, and is greater in compression than in tension. Therefore, when a pure moment is applied about the axis of a sealant joint, it will deflect in the manner sketched in Figure 5.

In order to determine the joint's rotational stiffness, a first step is to develop an expression for the width of the tension zone, l. Because the joint is in static equilibrium, the total tensile force is equal to the total compressive force, so:

$$0 = \int_{x=-(B-l)}^{l} f\left(\frac{x}{l}\frac{\Delta g}{g}\right) dx. \tag{8}$$

The result may be used to determine l, and then the total moment for a given

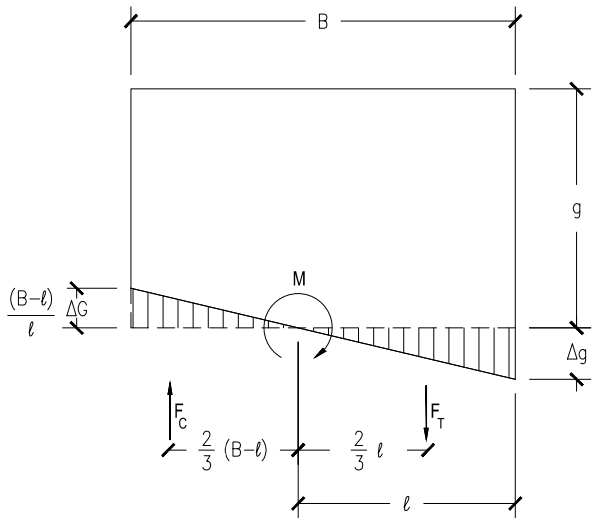

Figure 5: Cross section through structural sealant deflecting solely because of a moment about the joint's axis, with asymmetric tension and compression zones (cf. Figure 3). The positions of equivalent concentrated forces are based on the premise that Young's modulus is constant in the tension zone and constant in the compression zone.

Δg can be found by integration:

$$M = \int_{x=-(B-l)}^{l} xf\left(\frac{x}{l}\frac{\Delta g}{g}\right)dx. \tag{9}$$

When the sealant's stress-strain curve is given in polynomial form, as in Equation 5, mathematical integration is easy. However, the results cannot readily be reduced to a simple closed-form algebraic formula relating rotation to moment. What is needed is an approximation that can be expressed simply, and which is, at the same time, less crude than the model proposed in Section 2.

In the analysis that follows, it is assumed that a constant modulus of elasticity, E_{ss}, applies throughout the tension zone, and that its value is independent of strain. It is also assumed that the modulus of elasticity within the region that is in compression, E_C, is constant for any given angle of joint rotation, but it's value increases with rotation. The applicability of this set of assumptions is discussed in Section 7.1.

Applying these new premises to the sealant joint shown in Figure 5, the equivalent concentrated force in the triangular tension zone, F_T, and in the triangular compression zone, F_C, can be found in the same way that they were found for Equation 1. Static equilibrium is achieved when $F_T + F_C = 0$, hence:

$$\frac{l}{2}\frac{\Delta g}{g}E_{ss} + \frac{-(B-l)}{2}\frac{(B-l)}{l}\frac{\Delta g}{g}E_C = 0, \tag{10}$$

which reduces to:

$$\frac{E_{ss}}{E_C} = \frac{(B-l)^2}{l^2}. \tag{11}$$

By definition, if ε is a tensile strain, and if f is a stress function similar to Equation 5 or 6:

$$E_{ss} = \frac{f(\varepsilon)}{\varepsilon}. \tag{12}$$

The strains on the compression side are smaller in magnitude than those on the

tension side, and ε is a tensile strain, so:

$$E_C = \frac{-f\left(\frac{(B-l)}{l}\varepsilon\right)}{\frac{(B-l)}{l}\varepsilon}. \tag{13}$$

Substituting the above two expressions, for E_{ss} and E_C in Equation 11, and simplifying:

$$f(\varepsilon) = -f\left(\frac{-(B-l)}{l}\varepsilon\right)\frac{(B-l)}{l}. \tag{14}$$

The way in which the width of the tensile zone varies with strain has been determined numerically, using Equation 14, and the results are presented in Figure 6. The graph shows that, at the limit of allowable strain, when $\Delta g/g = 0.25$, which is the condition that will be of greatest interest to designers, $(B-l)/l \simeq 0.78$, which is to say that $l \simeq 0.56B$.

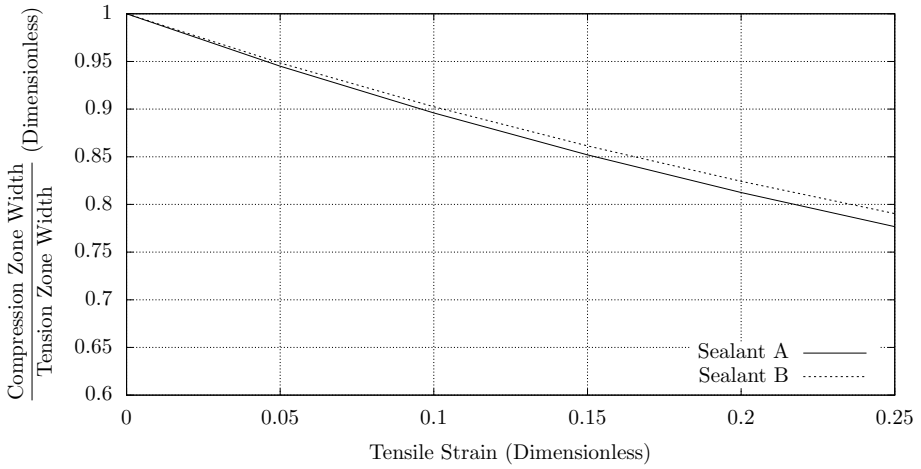

Figure 6: Width of the compression zone, as a proportion of the width of the tension zone, in a structural sealant joint subject to axial moment. Using the variable names shown in Figure 5, this is $(B-l)/l$.

The modified versions of Equations 1 and 3, for force and moment, are:

$$F_T = -F_C = \frac{l}{2}\frac{\Delta g}{g}E_{ss} \tag{15}$$

and,

$$M = \frac{Bl}{3}\frac{\Delta g}{g}E_{ss}. \tag{16}$$

When the glass edge rotation is α then, from Figure 5, $\alpha = \Delta g/l$, where α is less than 0.176 radians. Equation 16 now can be rewritten:

$$M = \alpha\frac{Bl^2E_{ss}}{3g}. \tag{17}$$

4. Experimental Method & Results

Three identical samples of structural silicone sealant were prepared specifically for this study. In each sample, DC-983 sealant was applied between two painted aluminium extrusions, to create a joint in which the thickness of the joint or "glueline", g, was 6 mm. The sealant joint was orientated with its axis perpendicular to the axis of the extrusions, as shown in Figure 7: the width of the contact surface between the sealant and the painted metal substrate or "bite", B, was 24.2 mm, and the joint's length was 110 mm. The glazing tape, seen in Figure 7, was not removed: it remained in place throughout the test process.

The thickness of the metal in the extruded aluminium box sections was sufficiently great – approximately 7 mm – that the magnitude of deflections occurring within the metal parts during testing was negligible.

DC-983 is available in two colors, gray and black, and the two varieties have different physical properties [20]. The samples used in this study were black.

After the sealant samples had been created, and during the periods between tests, they were stored in a covered outdoor location where they were not exposed to rain or direct sunlight. There, the ambient temperature varied between 20°C and 36°C, and the relative humidity ranged from 65 % to 85 %. Commentary in Section 6 considers the effect that environmental conditions have upon the sealant's physical properties.

For each test, one of the sample's two extrusions was clamped to a rigid support as indicated in Figure 7. A counterbalance was positioned so that the

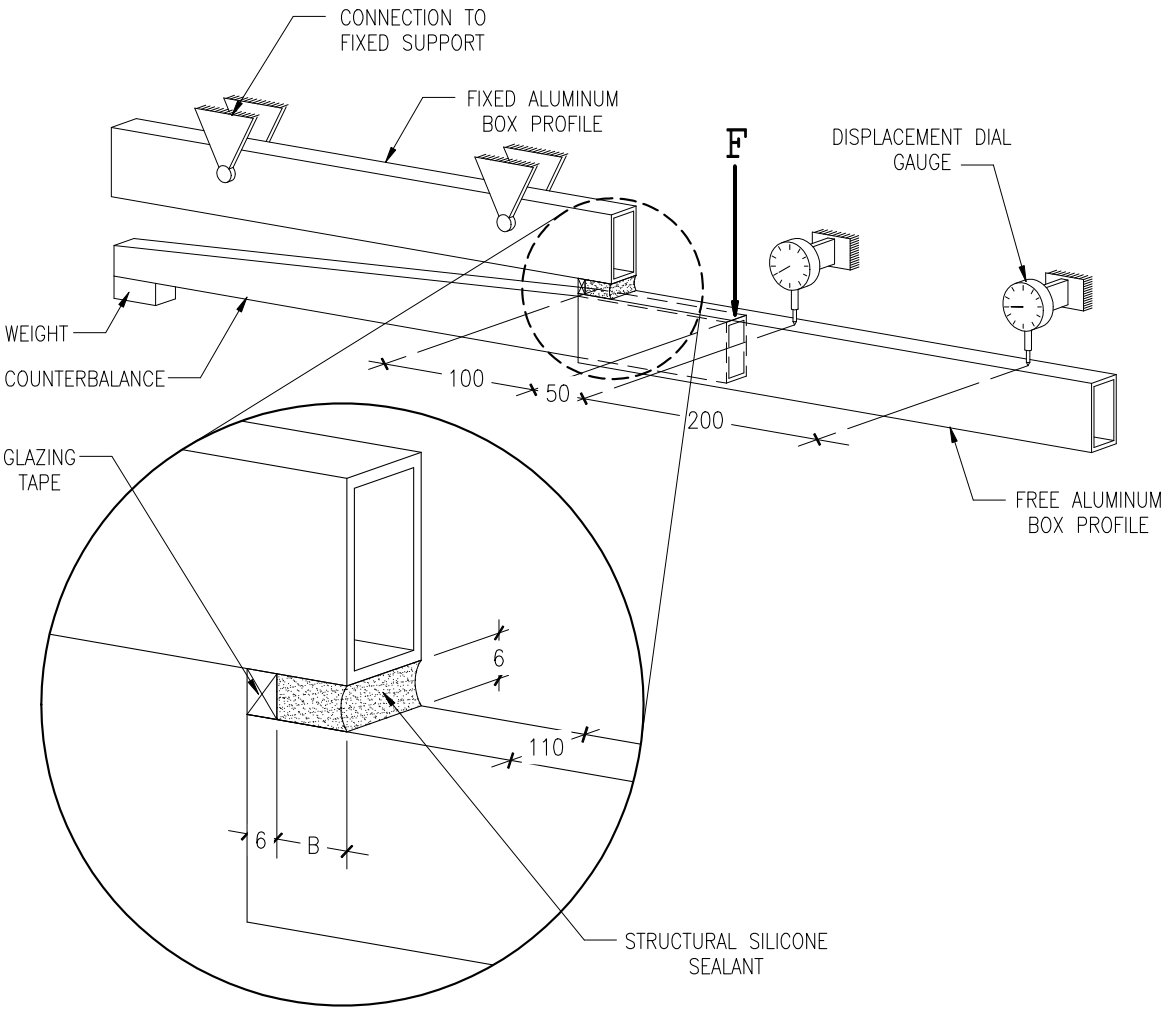

Figure 7: Experimental apparatus used to measure rotation of structural sealant joint with respect to applied moment. The box section on the left is rigidly fixed, while that on the right is supported only by the structural sealant sample. Load F is applied to the free side, while deflection is measured using dial gauges.

axis of the suspended extrusion, which was supported only by the structural silicone joint, was also horizontal. The load, which varied as a function of time, was applied to the suspended extrusion, at a distance of 100 mm from the sealant joint's centreline. Force was increased by 3.2 N every 30 seconds until the free beam's deflection was near to the maximum that the instruments could measure, or until the strain in the sealant was near to the 25 % limit established by the sealant's manufacturer [20]. Thereafter, force was removed incrementally, at the same rate as it had been applied. Immediately prior to each change in load, the position of the moving side of the sample was measured using dial gauges, graduated in hundredths of a millimeter, located as shown in Figure 7.

Each of the three sealant specimens was held and loaded, in sequence, in four different orientations, as shown in Table 1. Therefore, on each of the occasions that the samples' properties were measured – after 14, 114 and 214 days – the test procedure described above was carried out twelve times in total.

Figure 8 shows the magnitude of rotation about the axis of the sealant joint, plotted against applied moment, for two example sets of data – test numbers 9 and 10. The readings presented are those recorded while the load was being increased and while the load was being reduced. The hysteresis patterns are typical of those seen in the other test results.

The measurements plotted in Figure 9-A are similar – rotation with respect to moment – but records of all 12 tests carried out on the fourteenth day are presented. For clarity, the part of each sample's response that has been plotted is that recorded during the initial phase of the test, while the applied load was increasing. Figure 9-B is the mean tensile stress, averaged over the sealant joint's contact area, caused by the applied load together with the dead load of the suspended part of the test sample and its counterbalance. At any given test load, the magnitude of this direct stress is much less than the stress caused by the applied moment. The graph showing direct stress, Figure 9-B, has been provided beneath the rotation-moment plot so that the description of stresses is complete. This information may be of interest because, even though this paper's models presume that the relationship between stress and strain is linear, it is

	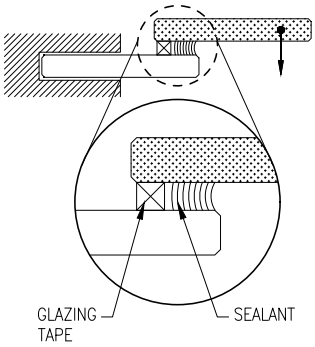	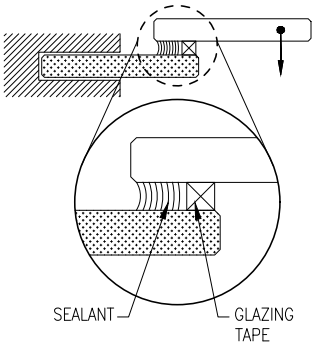
Simulating positive wind pressure.	Sample 1, Test 1 Sample 2, Test 5 Sample 3, Test 9	Sample 1, Test 4 Sample 2, Test 7 Sample 3, Test 11
	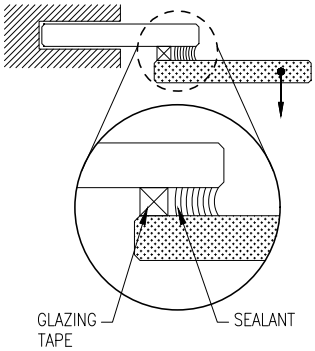	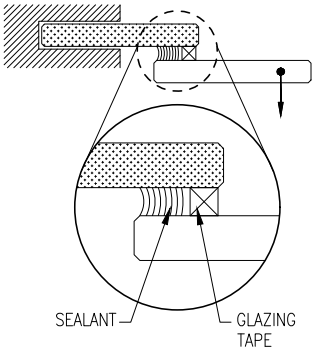
Simulating negative wind pressure.	Sample 1, Test 2 Sample 2, Test 6 Sample 3, Test 10	Sample 1, Test 3 Sample 2, Test 8 Sample 3, Test 12

Table 1: In a series of twelve tests, each of the three sealant specimens was tested in four different orientations. To make it easier to differentiate the two box sections, one has been drawn with shading. The enlarged views show the position of glazing tape in the joint.

known [22] that the elasticity of a structural sealant does, in reality, vary with stress.

When the sample's fixed beam was positioned below its free beam, which was the case during tests 1, 4, 5, 7, 9 and 11 (see Table 1), the counterbalance was not of the same length and mass as that used during the other tests. Hence, the absolute magnitudes of mean tensile or compressive stresses in the sealant during tests 1, 4, 5, 7, 9 and 11 were lower than those during other tests.

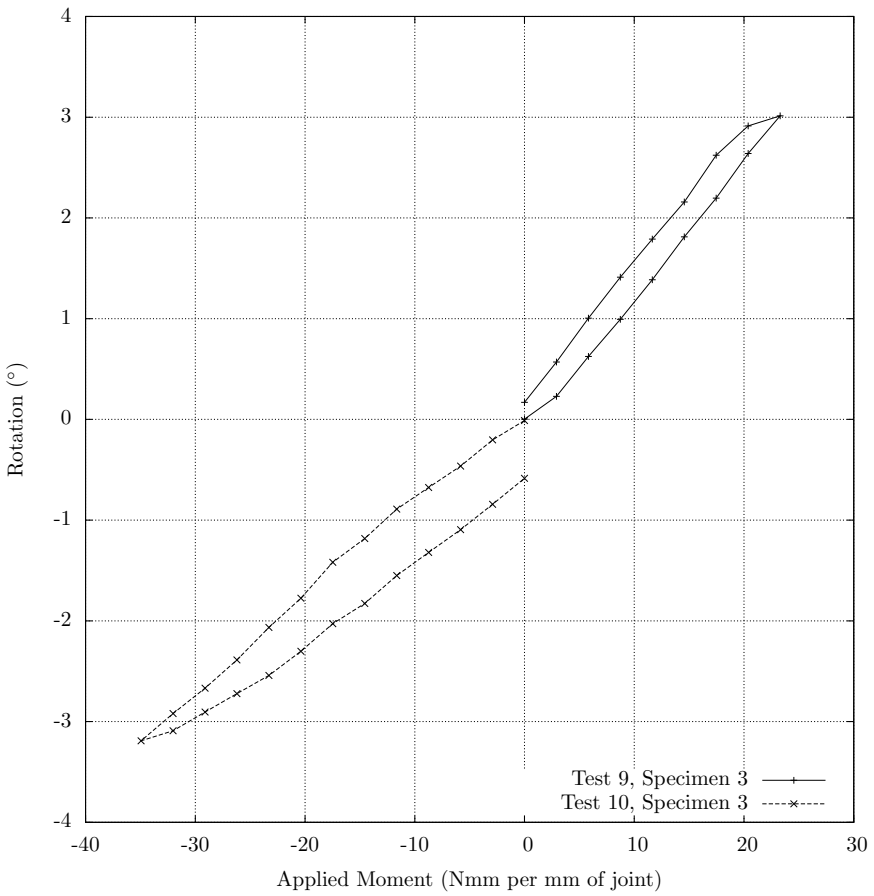

Figure 8: Rotation, as a function of the moment applied during tests 9 and 10, fourteen days after creation of the sealant samples.

The sequence of tests was repeated one hundred days later, on day 114, and then repeated again after a further one hundred days, on day 214. These two

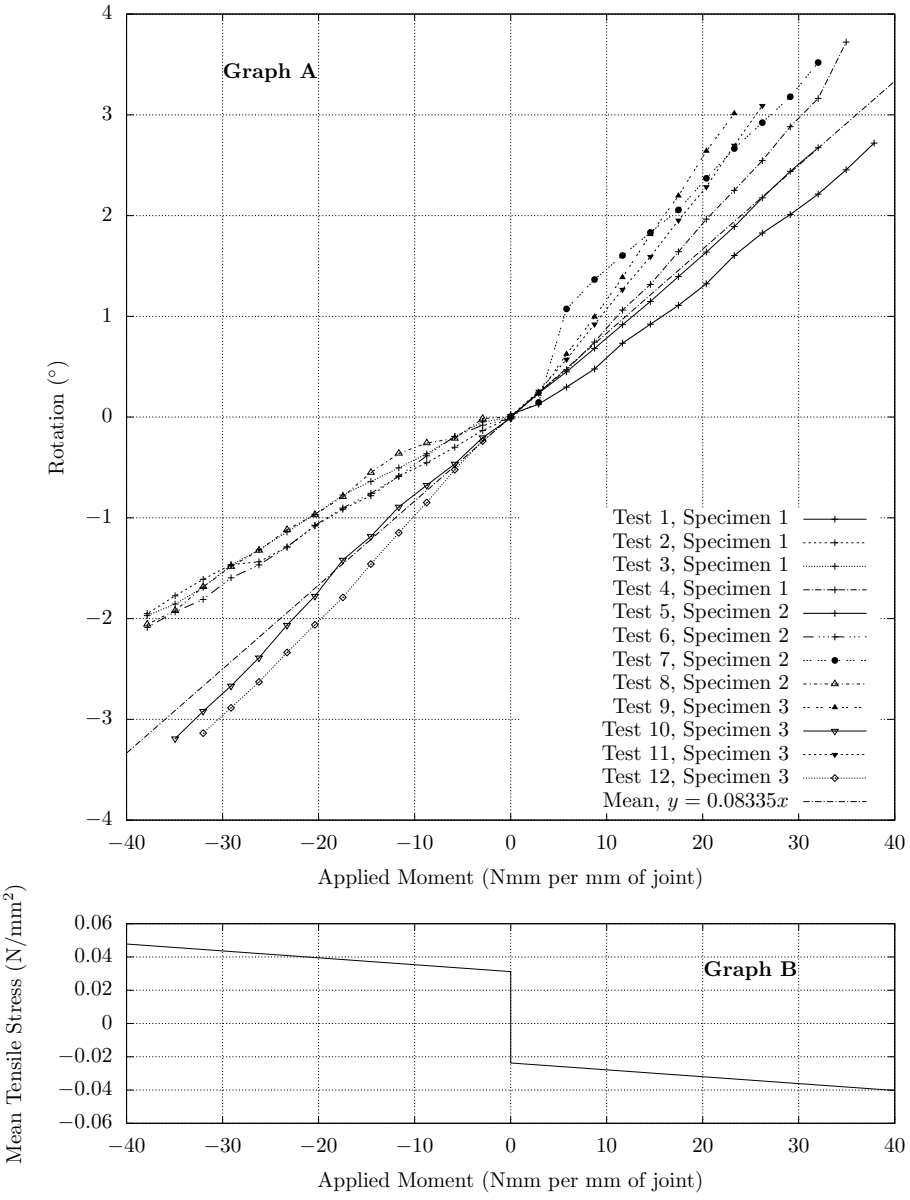

Figure 9: (Graph A) Rotation with respect to applied moment, measured 14 days after creation of the sealant joint, for each of the twelve test cases. (Graph B) Mean direct stress, averaged over the sealant-to-substrate surface area.

sets of rotation measurements, plotted against applied moment, are shown in Figures 10-A and 11-A respectively. For completeness, the corresponding direct stresses are given in Figures 10-B and 11-B.

In summary, the torsional resistance of sealant joints has been measured in the laboratory. Each of three specimens was tested in four different orientations, as shown in Table 1, after 14, 114 and 214 days. All 36 measured rotational stiffness are presented, in the form of a histogram, in Figure 12.

5. Young's Modulus of Structural Silicone Sealant

After rotational resistance had been measured for the third time, on day 214, each specimen was partially disassembled by separating the sealant from one of its metal substrates using a sharp blade. At the newly-exposed surfaces of sealant and glazing tape, hardness was found using a Shore A indentation tester [23, 24]. For each of the three specimens, sealant hardness measurements were taken at six locations. For specimens 1 and 2, glazing tape hardness measurements were taken at six locations. As the glazing tape in specimen 3 had been damaged when it was separated from its substrate, it was possible to measure its hardness in only one location. Minimum, mean and maximum values are shown in Table 2. Because the thickness of material tested was equal to the sealant joint's glueline, 6 mm, it was not necessary to apply any correction to the gauge readings [25, Figure 3]. As the glazing tape is narrow – only 6 mm in width – the centre of the tip of the indentation tester could not be positioned more than 3 mm from the tape's edge. The close proximity of the indenter to the edge is likely to have influenced the measurements but, as discussed in Section 7.3, the tape's properties are not considered in this paper's algebraic models of sealant joint behaviour.

The behaviour of an elastic material under the tip of a hardness instrument's indenter was considered by Gent [26], who proposed the following theoretical

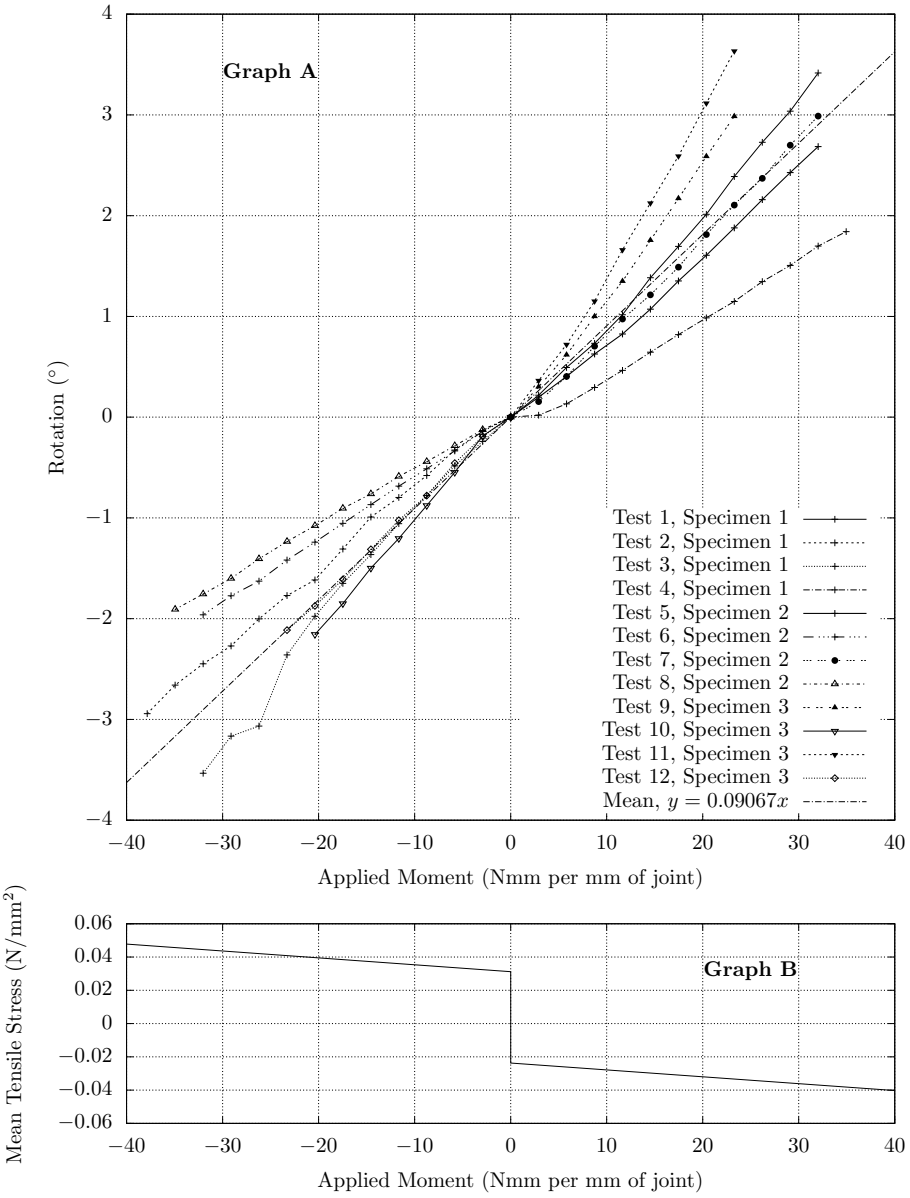

Figure 10: (Graph A) Rotation with respect to applied moment, measured 114 days after creation of the sealant joint, for each of the twelve test cases. (Graph B) Mean stress, averaged over the sealant-to-substrate surface area.

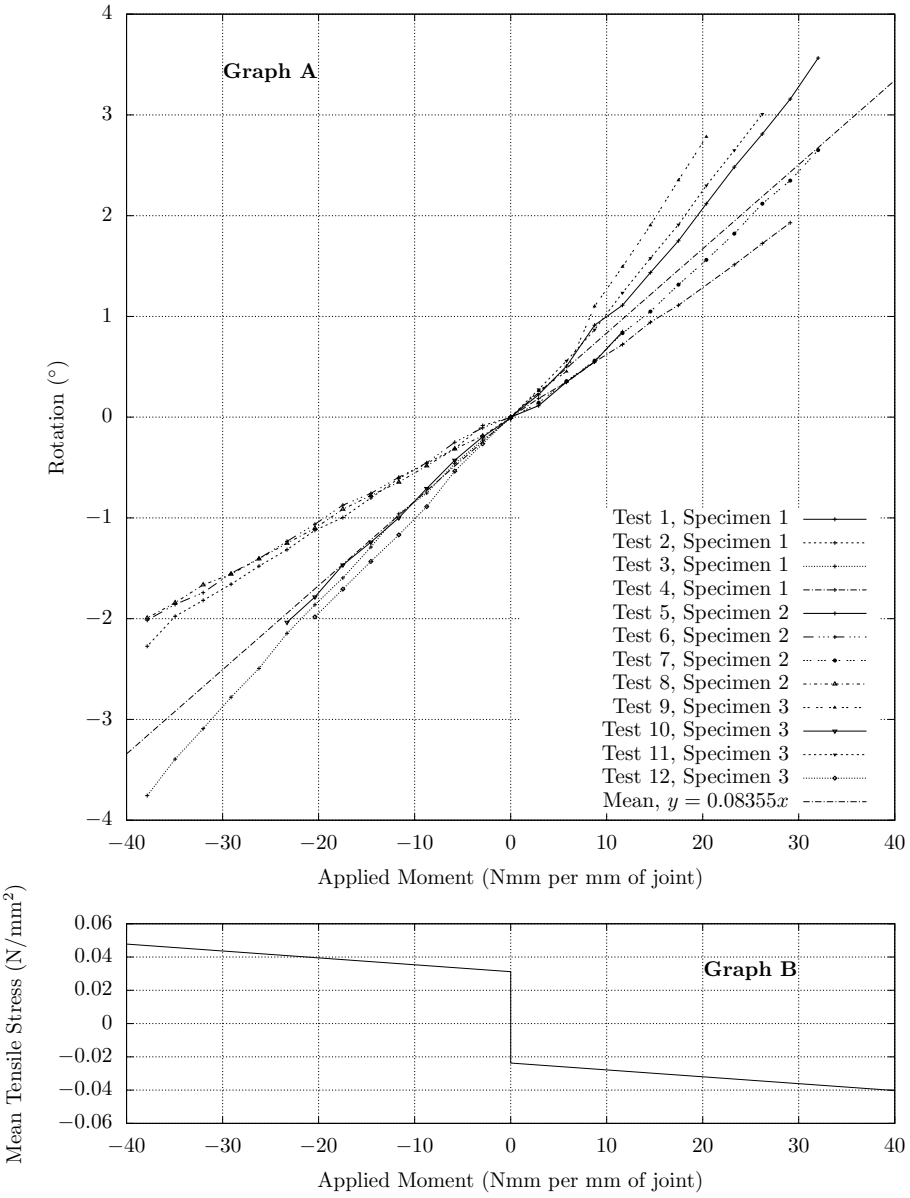

Figure 11: (Graph A) Rotation with respect to applied moment, measured 214 days after creation of the sealant joint, for each of the twelve test cases. (Graph B) Mean stress, averaged over the sealant-to-substrate surface area.

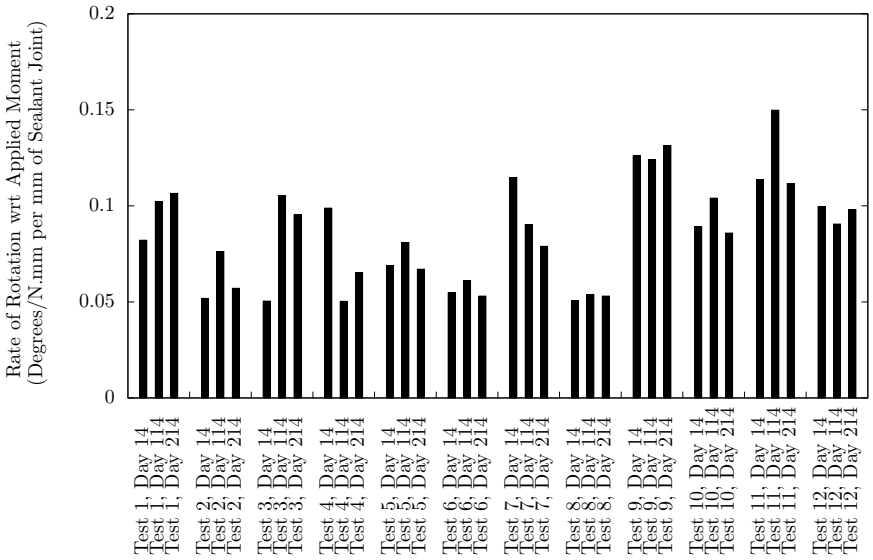

Figure 12: The torsional resistances of three structural silicone sealant specimens, were measured in four different orientations (Table 1), after 14, 114 and 214 days. The experimental results are presented in this histogram. Rotational stiffnesses are the gradients of straight lines fitted to the test results shown in Figures 9, 10 and 11, and the units are degrees of rotation per N.mm of applied moment, per mm of axial length of sealant joint.

Material Tested	**Specimen Number**	**Shore A Hardness**		
		Min.	Mean	Max.
Structural sealant.	1	34	**35.3**	38
Structural sealant.	2	32	**33.2**	34
Structural sealant.	3	34	**34.5**	36
Glazing tape.	1	30	**31.2**	35
Glazing tape.	2	21	**25.3**	28
Glazing tape.	3	32	**32.0**	32

Table 2: Hardness of the DC-983 structural sealant samples, as well as the hardness of the glazing tape, measured with a Shore A indentation gauge 214 days after creating the specimens.

relationship between Young's modulus, E, and Shore A hardness, S;

$$E = \frac{0.0981(56 + 7.62336S)}{0.137505(254 - 2.54S)} \,. \tag{18}$$

In various studies documented in the existing literature, for a wide range of different materials, values of Young's modulus determined by tensile testing have been compared with values based on indentation hardness measurements. Regression analysis of the laboratory data [e.g. 27] has shown that, away from the extreme ends of the hardness scale, the relationship between Young's modulus and Shore A hardness is in close agreement with that predicted by Gent (Equation 18). There is however significant scatter in the experimental data, and for this reason values of Young's modulus derived from individual indentation hardness measurements should be considered to be indicative rather than precise.

According to the manufacturer's technical data sheet [20], the hardness of the sealant used in this study, DC-983, should be in the range between 35 and 45 on the Shore A scale. Gent's conversion method, Equation 18, implies that the Young's modulus will be in the range between 1.39 and 2.03 MPa.

The different estimated values for the Young's modulus of the DC-983 sealant samples tested in this study, obtained by the methods outlined in this section, are summarized in Table 3.

6. Discussion of Experimental Findings

It is known that the apparent elasticity of a viscoelastic material varies with the magnitude of strain, strain rate and the direction of loading [for structural sealant, see 22], and it is therefore to be expected that any quantification of Young's modulus will be influenced by the manner in which measurement is made. In Table 3, the values of Young's modulus in the second and third rows have been obtained from tensile tests, those in the first and last rows are based on indentation hardness measurements, while the estimates in the fourth and fifth rows are those implied by the rotational stiffness equations that were

Basis for Estimate	**Age**	**Shore A Hardness**			**Implied Young's Modulus**		
		Min.	Mean	Max.	Min.	Mean	Max.
	Days				N/mm^2	N/mm^2	N/mm^2
Sealant manufacturer's published Shore A range [20], converted to Young's modulus using Equation 18.	7	35	-	45	1.39	**1.71**	2.03
Young's modulus implied by sealant manufacturer's published stress at 10 % strain [20].	21	-	-	-	-	**2.00**	-
Linear elastic model based on laboratory tension measurements [19] at up to 25 % strain (Figure 2).	21	-	-	-	-	**1.60**	-
Mean measured joint stiffness (Figures 9, 10 & 11) converted to Young's modulus using Equation 4.	14	-	-	-	2.31	**3.49**	5.77
	114	-	-	-	1.94	**3.21**	5.79
	214	-	-	-	2.22	**3.48**	5.49
Mean measured joint stiffness (Figures 9, 10 & 11) converted to Young's modulus using Equation 17.	14	-	-	-	1.83	**2.76**	4.56
	114	-	-	-	1.54	**2.54**	4.57
	214	-	-	-	1.75	**2.75**	4.34
Measured Shore A hardness (mean of values in Table 2) converted to Young's modulus using Equation 18.	214	32	34.3	38	1.24	**1.36**	1.57

Table 3: Different estimated values of Young's modulus for the DC-983 structural silicone samples tested in this study.

developed in Sections 2 and 3. Therefore it is true that, here, apples have not been compared with apples. However, the following observations can be made:

(a) The behavioural model that underlies the estimates in the fourth row of Table 3, that is the basis for Equations 3 and 4, assumes that the relationship between stress and strain is the same whether the sealant is in tension or compression. The result of this simplification – that is to say, ignoring the increase in elastic modulus that occurs when the sealant is in compression – is an increase in the sealant's apparent elastic modulus in tension.

(b) Taking laboratory measurements of rotation with respect to moment, and finding the elastic moduli that are implied by the asymmetric tension-compression model that is the basis for Equation 16, leads to the values shown in the fifth row. The mean of these implied elastic moduli is $2.68\,\mathrm{N/mm^2}$, which is, in comparison to the elastic moduli obtained using Equations 3 and 4, closer to the value published by sealant manufacturer ($2.00\,\mathrm{N/mm^2}$, in the second row of Table 3).

As noted previously, the sealant samples were cured, stored, and tested in conditions ranging between 20°C and 36°C, and 65 % to 85 % relative humidity. This environment was therefore warmer and more humid than the reference conditions – a constant 25°C and 50 % relative humidity – in which the sealant manufacturer's own test specimens cured [20]. The manufacturer indicates [also 20] that elevated temperatures do increase the rate of curing, but published test results [28, Table 1] suggest that the impact of the non-standard storage temperature and humidity upon the modulus of elasticity of this particular sealant, DC-983, is small. Also, it should be remembered that any deviation from the ideal laboratory conditions has been modest in comparison with the extremes that are experienced by structural sealants in service, where facade surface temperatures of -20°C through +80°C can be encountered.

7. Validity of the Mathematical Model

The rotation of an idealized structural sealant joint can be predicted using Equation 3. In this model, the relationship between stress and strain in the sealant is linear, and the glazing tape, shown in Figures 1-B, 1-D and 7, does not affect the moment resistance. It is worth revisiting these two premises in the light of the experimental findings.

7.1. Variability of the Sealant's Apparent Modulus of Elasticity

The algebraic model presented in Section 2 is based upon the assumption that structural sealant obeys Hooke's law. However, it has been noted already that actual stresses, measured in conditions of steadily increasing strain, differ from the linear-elastic ideal by around 9 % in the range of strain between zero and 25 %. Further deviation from the theoretical model is to be expected in service, where, in wind storms, the rate of change in pressure or the duration of load application might differ greatly from this study's conditions. In addition, the material's elastic modulus may be influenced by its cyclic loading history [29]. In short, a structural designer should be aware that the effective value of a structural sealant's Young's modulus may vary with factors such as age, temperature and loading history, and the range may be a large proportion of the mean. This is not to say, however, that a structural sealant cannot function effectively as a restraint for the metal member to which it is bonded.

The mathematical representations of rotational resistance are based upon premises that are not perfectly consistent with each other. For example, in Section 3, the modulus of elasticity on the compressed side of joint is assumed to vary with glass rotation but, at the same time, it is assumed that elasticity at any given angle of rotation is constant within the triangular compression zone, even though strain varies in that region. There is therefore an element of arbitrariness in the formulation of the models. Rather than try to correct the inconsistencies or to create a more realistic and more complex model, a more practical approach might be to use an empirical constant to adjust the crude relationships, such as Equation 3, offered in Section2.

7.2. Influence of Sealant Joint's Cross Sectional Aspect Ratio

Normally, when a piece of incompressible or partially compressible solid is stretched in one direction, there is a reduction in the area of its cross section in the perpendicular plane. This, of course, is Poisson's effect. However, when sealant is bonded to a rigid substrate then, in the material adjacent to the contact surface, Poisson's stresses are resisted by the adhesive connection. Because changes in cross-sectional shape are inhibited in this way, in vicinity of the substrate, the sealant's effective elasticity is reduced. Changing the shape of a sealant joint therefore effects the material's apparent rigidity, E_r. As the ratio of bite to glueline or, using the variable names shown in Figures 3 and 5, B/g, increases, so the sealant's apparent rigidity will increase.

The value of a sealant's elastic modulus that is published by the product's manufacturer is, commonly, determined by the ASTM C1135 method [18], using sealant specimens with a bite to glueline ratio of 1:1. Laboratory tests have shown [30, p. 42] that changing the joint's aspect ratio from 1:1 to 2:1 "more than doubles" the apparent modulus of elasticity in a tensile test. Recently Descamps, Hayez and Chabih [31] studied the influence that aspect ratio has upon the rigidity of a particular, two-part, structural silicone sealant, DC-993, and they concluded that the relationship is described by the second order polynomial below;

$$E_r = \left[0.1506 \left(\frac{B}{g}\right)^2 + 0.3409\frac{B}{g} + 1.0852\right] E. \tag{19}$$

The expressions for a sealant joint's moment resistance, which were developed in Sections 2 and 3, can be modified to model the significance of joint shape by replacing Young's modulus, E, with the effective rigidity of the sealant, E_r, from Equation 19.

The modulus of elasticity of the structural sealant used in this present study's laboratory tests, DC-983, is similar to that of the product considered by Descamps et al. According to the technical data published by the manufacturer [32], the Shore A hardness of DC-993, measured after 7 days at 25°C and 50 % relative humidity, is 40, while that of the DC-983 [20] tested in this investigation

is in the range between 35 and 45. It might appear, therefore, that Equation 19 could be applied to this current analysis. However, if the sealant's modulus of elasticity is in the range between 1.36 and 2.0 MPa (see Table 3), then the modulus of rigidity of the joints tested in the laboratory (Section 4) will, from Equation 19, be in the range from 6.68 to 9.8 MPa. This range is well above the mean apparent value implied by the rotational stiffness test measurements, which is less than 3.5/,MPa (Table 3, row 4).

It remains reasonable to argue that the apparent modulus of elasticity based on torsional rigidity measurement is greater than the modulus of elasticity inferred from indentation hardness measurements because the sealant joint samples have a high bite to glueline ratio. However, Equation 19 was developed by Descamps and coauthors for the analysis of structural sealant joints in tension, and it appears to overestimate the rigidity of joint in which, as in this instance, the predominant load is torsion.

7.3. The Influence of Glazing Tape

The "glazing tape" adjacent to the sealant in the test specimens (see Figures 1-D & 7) is an open-cell foam spacer, square in cross-section, with acrylic adhesive on the two sides in contact with the substrates. Its purpose is to maintain the required distance between the bonding surfaces while the sealant is being applied and while it is curing but, as is the usual practice in glazing systems, the tape was not subsequently removed from the joint.

In the proposed mathematical models for the joint's rotational stiffness, established in Sections 2 and 3, the glazing tape has been ignored. When the load applied to the test specimens caused tension in the sealant beside the glazing tape – during tests 3, 8 and 12 (see diagram in Table 1) – it was obvious from inspection that the tape's adhesive held it to only one side of the joint, and the tape therefore played no part in the transfer of moment. This condition is outlined in the left hand diagram of Figure 13. Conversely, during tests 4, 7 and 11, the glazing tape was placed in compression, in the manner shown in the right side of Figure 13. However, the test results do not show a consistent increase

in the joint's rotational stiffness. The experimental data therefore support the assumption that the contribution of glazing tape can be ignored in analysis of moment resistance.

In some glazing systems, the material used to separate the metal and glass may be much harder than the glazing tape that has been used in this study. When such a separator is placed in compression, the deflected shape of the sealant joint will be similar to that shown in right hand diagram of Figure 13, except that the fulcrum for glass rotation might be at, or near to, the upper right hand corner of the sealant's initial, unloaded cross section. Here, all of the sealant is in placed in tension, and the joint's theoretical moment resistance can be determined using the expression below, which has been derived in the same way as Equation 4:

$$E_{ss} = \frac{3gM}{\alpha B^3}. \tag{20}$$

8. Quantifying Axial Moment in Framing Members

When a rectangular pane of glass is simply supported at its perimeter and subjected to a uniform pressure acting normal to its plane, the deflected shape

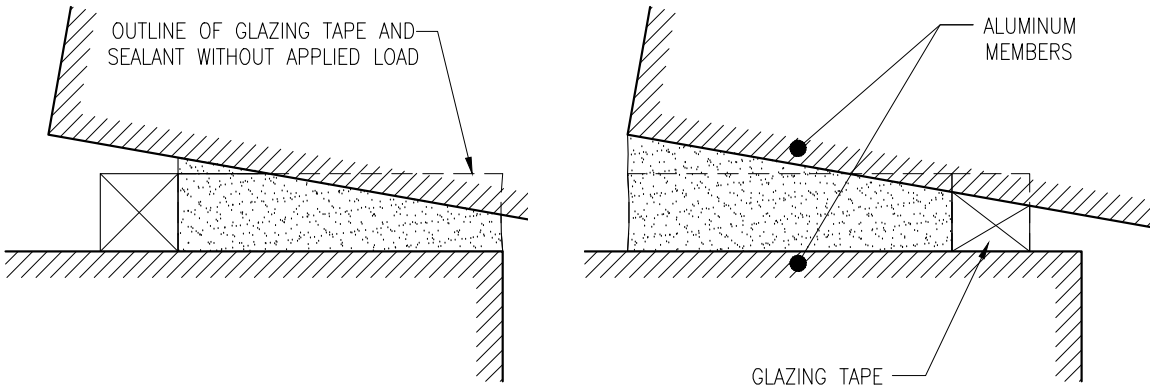

Figure 13: Glazing tape separates from one of its substrates when the adjacent sealant is in tension (Left). However, when the adjacent sealant is compressed (Right), the glazing tape also is placed in compression.

of its surface, measured along any line parallel to an edge, is similar to one half period of a sinusoid [33, Equation 36] if the sides of the pane are not greatly different in length. It is to be noted that this approach will under-estimate edge rotations away from the centre of the sides of plates with higher aspect ratios [34, Figures 56-71]. This point is best explained with reference to Figure 14, which shows the actual deflected shape of a rectangular plate with aspect ratio of three, and that shape's deviation from the sinusoidal idealization. At any point along the centreline parallel to the long sides, other than at the plate's geometric centre, the actual deflection exceeds the sinusoidal model's prediction.

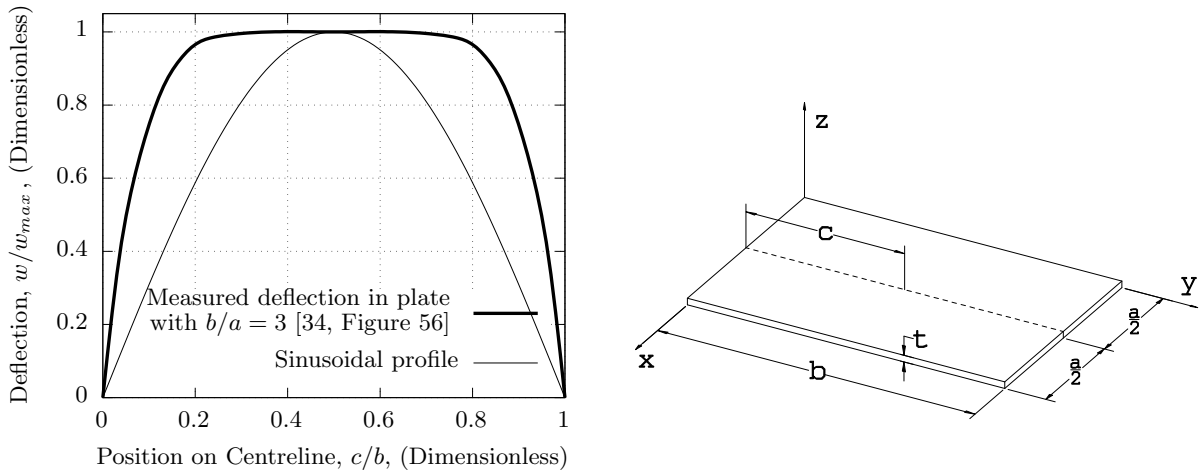

Figure 14: The graph's heavy line shows the deflected shape of an initially-flat rectangular plate with aspect ratio $b/a = 3$, measured at the centreline parallel to the long sides, when a uniform pressure is applied to the plate's surface [traced from 34, Figure 56].

Even though the actual rotations at both the long and the short edges of a rectangular plate will, if the plate's edges are disparate in size, be larger than those predicted by the sinusoidal surface model, the model is still useful because its mathematical description is simple. If the lengths of a panes' short and long sides are, respectively, a in the x direction and b in the y direction, if w_c is the central deflection, and if $w_{x,y}$ is the deflection at point (x, y), then an expression

for the sinusoidal surface is;

$$w_{x,y} = w_c sin\left(\frac{\pi x}{a}\right) sin\left(\frac{\pi y}{b}\right). \tag{21}$$

The gradient in the x-direction is obtained by differentiating partially;

$$\frac{\partial w_{x,y}}{\partial x} = \frac{\pi w_c}{a} cos\left(\frac{\pi x}{a}\right) sin\left(\frac{\pi y}{b}\right). \tag{22}$$

so, at the middle of the pane's longer side, where $x = 0$ and $y = b/2$;

$$\frac{\partial w_{x,y}}{\partial x} = \frac{\pi w_c}{a}. \tag{23}$$

As is evident in the diagram at the right hand side of Figure 3, the gradient of the glass surface at the sealant joint is $2\Delta g/B$. Substituting for gradient in Equation 23 gives;

$$\Delta g = \frac{\pi B w_c}{2a}. \tag{24}$$

In reality, when wind pressure acts upon a structurally glazed pane, the sealant at its perimeter experiences both a direct force and a moment. However, it is easiest to convey the relative importance of these two components of load if the force is considered to act, as shown in Figure 15, through an imaginary lever attached to the frame, at a distance e from the centreline of the sealant joint. The significance of a given eccentricity will be immediately apparent to curtain wall designers, who are accustomed to seeing similar lever arms in the shapes of brackets used to connect mullions to a building's primary structure.

In a structurally optimized design, the width of the sealant bite will be minimized so that the actual tensile stress is equal to the maximum allowable stress, F_t. So, considering a unit length of sealant joint and substituting for M in Equation 3;

$$F_t B e = \frac{B^2 \Delta g E_{ss}}{6g}, \tag{25}$$

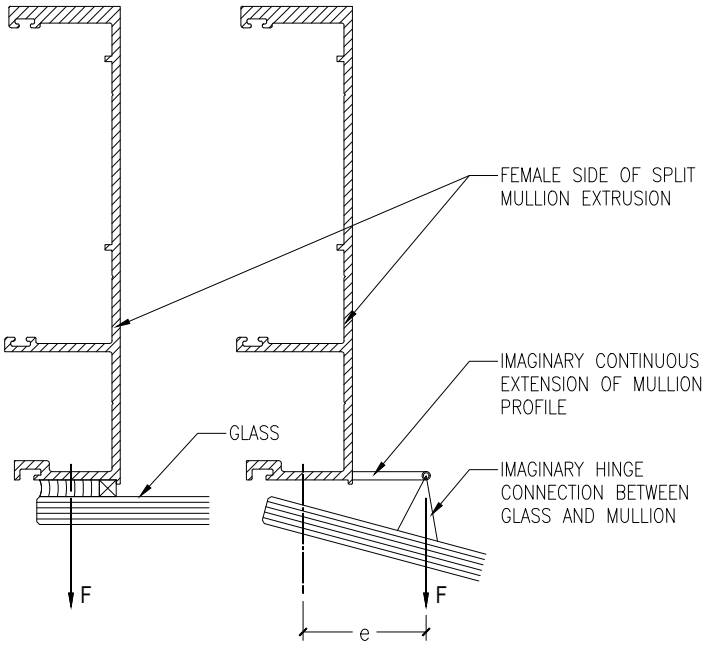

Figure 15: The current analytical convention is that loads transferred from glass to mullion are considered to act through the centre of the structural sealant *(Left)*, but in reality, because rotation occurs at the glass edge *(Right)*, there is an effective eccentricity, e, between the force and the sealant joint.

then substituting for Δg from Equation 24, and simplifying;

$$e = \frac{\pi B^2 E_{ss} w_c}{12 F_t a g}. \tag{26}$$

In practice, the maximum allowable glass deflection is often specified as a proportion of the length of the pane's shorter side. A limit commonly found in design codes and technical specifications for glazing – for example, the Australian design code for glass in buildings [35, Section 3.3.3] – is $w_c = a/60$. At this deflection condition, Equation 26 becomes;

$$e = \frac{\pi B^2 E_{ss}}{720 F_t g}. \tag{27}$$

Typical numerical values can be assigned to the variables in Equation 27 in order to assess whether the magnitude of the turning moment – that imparted by the glass, through the structural sealant, to the glazing system's metal frame – is of practical significance. Assuming that the structural sealant industry's standard tensile stress limit is observed, $F_t = 139\,\text{kPa}$ [5, Section 27.5], and that the geometry and elastic modulus of the joint are similar to those in the samples that were tested in this study, with glueline $g = 6\,\text{mm}$, bite $B = 22.5\,\text{mm}$, and $E_{ss} = 4.0\,\text{MPa}$ (see Table 3), then the eccentricity of the load, e, measured from the joint's centreline, is 10.6 mm. The effect of the moment upon the glazing frame will of course depend upon the cross-sectional shape and span of the mullion profile, but it is probable that, in most cases, an eccentricity of this magnitude could safely be neglected by the framing designer. However, if the sealant's elastic modulus were to be at the upper end of the range that has been observed in one-part structural silicones, say $E_{ss} = 20.0\,\text{MPa}$ [e.g. 17, Figure 6], then the value of e would be 53.0 mm. Such a large eccentricity certainly would concern the designer of a typical unitized curtain wall system with open, E-shaped mullion extrusions.

9. Conclusions

When wind load causes the glass or other sheet infill material at the face of a structurally glazed curtain wall to deflect, moments are induced about the longitudinal axes of the framing members.

Using the analytical methods proposed in this paper, facade engineers can incorporate mathematical expressions – for a sealant joint's rotational stiffness and, hence, for axial moment – in their structural models of curtain wall mullions. There are at least two practical incentives to do so. Firstly, it will be possible to identify, during the design process, cases in which excessive axial rotation of a proposed mullion extrusion would impair its non-structural functions, such as the effectiveness of its air seals. Secondly, if analysis shows that the torsional restraint provided by a sealant-to-glass connection is sufficient to prevent lateral torsional buckling, then there will be an opportunity to create framing members containing less aluminium than would be needed if the established structural design conventions were to be observed. For this second application, however, further research into the stability of structurally glazed members will be needed to demonstrate that they can be reliably restrained by structural sealant in the all of the conditions that might be experienced by the facades of real buildings.

Data sets have been obtained by physical testing and the results show that, for any one sample sealant joint, the relationship between rotation and applied moment is practically linear. The variation between one sample and another is, however, considerable: in a population of sealant joints, one standard deviation is approximately one third of the mean value. So, when estimating the magnitude of the moment transferred to the frame of a structurally glazed pane, a pragmatic approach will be to consider a range of values for the sealant joint's stiffness. When establishing that range, it should be kept in mind that the variability in rotational stiffness of structural sealant joints in a real building's curtain wall panels will, because of normal batch-to-batch inconsistencies in the sealant properties, dimensional tolerances, differences in loading history

and other factors, be greater than that observed in these tests, which have been carried out in relatively tightly controlled conditions.

The hardness of this study's sealant samples, measured by the indentation method (Table 3, last row), was found to lie within the range published by the sealant manufacturer (Table 3, first row). However, the mean value of this study's laboratory measurements of rotational stiffness, when used with the simple mathematical model proposed in Section 2, suggests that the elastic modulus of the sealant samples (Table 3, fourth row) is approximately 70 % greater than the value published by the sealant manufacturer (Table 3, second row). The more refined behavioural model, laid out in Section 3, which acknowledges a difference between the sealant's properties in tension and compression, also leads to a value of Young's modulus that is an apparent overestimate: the computed value (Table 3, fifth row) is about 34 % greater than that indicated by the sealant manufacturer (Table 3, second row). Nonetheless, even if predictions of rotational stiffness based upon this paper's algebraic models are not in precise agreement with the laboratory results, the models are still useful to facade designers. Providing the analysis of an adhesive joint's rotational stiffness will take into consideration a suitably wide range of possible values for the structural sealant's elastic modulus, some degree of inaccuracy in the predictive model will not be of consequence.

Others [17] have recorded a manyfold increase in the Young's modulus of single-part structural silicone sealant, occurring during the months after the initial fortnight of curing. The DC-983 two-part sealant specimens prepared for this investigation were tested at 14, 114 and 214 days, but no significant change in modulus was observed. This observation shows that, at 14 days, the cross-linking of polymer chains within the sealant – the curing process – was complete or substantially complete.

Using the formulae that have been presented in this paper, designers of curtain wall systems will be able to estimate quickly, without a requirement for numerical modelling, load eccentricities that are ignored in standard structural analyses. The information will be of greatest interest when the metal framing

members to which structural glazing is to be applied are susceptible to rotation about their longitudinal axes – for example, if unsupported spans are long, and if the profiles have low torsional rigidity.

10. Acknowledgements

The authors are grateful to Mr. James Chant, Chairman of Seapac Philippines Inc., who provided the material samples used in these tests. Mr. Lawrence Carbary of Dow Corning reviewed a draft of this paper and made helpful comments. Staff of PTCC Facade Design, led by Engineer Warren Tan and Mr. Rene Ramiscal helped to commission the test rig and collect data. PTCC's Mr. Jhun Fabrero transformed the authors' hand sketches into CAD drawings.

References

[1] Yeomans D. The pre-history of the curtain wall 1998;14:59–82. URL: http://www.arct.cam.ac.uk/Downloads/chs/final-chs-vol.14/chs-vol.14-pp.59-to-82.pdf.

[2] Ábalos I, Herreros J. Tower and Office: From Modernist Theory to Contemporary Practice. MIT Press; 2003. ISBN 0-262-01191-3.

[3] Yeomans D. The origins of the modern curtain wall. APT Bulletin 2001;32:13–8. URL: http://www.jstor.org/stable/1504688. doi:10.2307/1504688.

[4] Murray S. Contemporary Curtain Wall Architecture. Princeton Architectural Press; 2009. ISBN 978-1-56898-797-2.

[5] ASTM C1401. Standard Guide for Structural Silicone Sealant Glazing; 2014. doi:10.1520/C1401-14.

[6] American Architectural Manufacturers Association. Curtain Wall Design Guide Manual; 2005.

[7] Watts A. Modern Construction Envelopes. 2 ed.; AMBRA — V; 2014. ISBN 978-3-99043-559-5.

[8] Yuanda China Holdings Limited. Global Offering; 2011. URL: www.hkexnews.hk/listedco/listconews/sehk/2011/0420/02789_1057382/EWF114.pdf; (Document available from Hong Kong Stock Exchange).

[9] Ziemaian RD, editor. Guide to Stability Design Criteria for Metal Structures. 6 ed.; John Wiley & Sons; 2010. ISBN 978-0-470-08525-7.

[10] Center For Window and Cladding Technology. Technical Update No. 7: Buckling of Curtain Wall Mullions; 2002.

[11] Aluminum Association. Aluminum Design Manual; 2005.

[12] Goco LT. Rationalizing assumptions for evaluating the lateral torsional buckling strength of aluminium mullion extrusions by EN1999 and AA ADM. Master's thesis; Bath University, UK; 2017. URL: https://www.bath.ac.uk/library/dissertations/index.php?programme=MSc+Architectural+Engineering%3A+Faade+Engineering.

[13] Skejić D, Lukić M, Buljan N, Vido H. Lateral torsional buckling of split aluminium mullion. Key Engineering Materials 2016;710:445–50. doi:10.4028/www.scientific.net/KEM.710.445.

[14] Clift CD, Austin WJ. Lateral buckling in curtain wall systems. Journal of Structural Engineering 1989;115(10):2481–95. doi:10.1061/(ASCE)0733-9445(1989)115:10(2481).

[15] Hammond G, Jones C. Embodied Carbon: The Inventory of Carbon and Energy (ICE). Bath University and BSRIA; 2011. ISBN 978 0 86022 703 8.

[16] Lee AD, Shepherd P, Evernden MC, Metcalfe D. Optimizing the architectural layouts and technical specifications of curtain walls to minimize use

of aluminium. Structures 2017;13:8–25. doi:10.1016/j.istruc.2017.10.004.

[17] Ramesh K, Tock RW, Narayan RS, Vallabhan CVG. Property evaluation of silicone elastomers used in tension-adhesion joints. Materials and Science Letters 1995;14:964–7. doi:10.1007/bf02427478.

[18] ASTM C1135. Standard Test Method for Determining Tensile Adhesion Properties of Structural Sealants; 2015. doi:10.1520/C1135-15.

[19] Kimberlain J, Carbary L, Clift CD, Hutley P. Advanced structural silicone glazing. International Journal of High-Rise Buildings 2013;2(4):345–54.

[20] Dow Corning Corporation. Product Information: Dow Corning 983 Structural Glazing Sealant; 2012. URL: http://www.dowcorning.com/content/publishedlit/63-1110.pdf; Dow Corning Form Number: 63-1110C-01.

[21] Vallabhan CVG, Aşik MZ. Analysis of structural glazing systems. Computers and Structures 1997;65:231–9. doi:10.1016/S0045-7949(96)00284-2.

[22] Wolf AT, Cleland-Host HL. Material properties for use in FEA modeling: Sealant behaviour with ambient laboratory climate aging. Journal of ASTM International 2004;1(7):372–84. doi:10.1520/JAI11603.

[23] ASTM C661. Standard Test Method for Indentation Hardness of Elastomeric-Type Sealants by Means of a Durometer; 2011. doi:10.1520/C0661-06R11.

[24] ASTM D2240. Standard Test Method for Rubber Property – Durometer Hardness; 2005. doi:10.1520/D2240-05R10.

[25] Casa L, Mendichi R. Shore A hardness and thickness. Polymer Testing 1986;7:165–75. doi:10.1016/0142-9418(87)90030-4.

[26] Gent AN. On the relation between indentation hardness and Young's modulus. Rubber Chemistry and Technology 1958;31(4):896–906. doi:10.5254/1.3542351.

[27] Larson K. Can You Estimate Modulus From Durometer Hardness for Silicones?; 2016. URL: http://www.dowcorning.com/content/publishedlit/11-3716-01_durometer-hardness-for-silicones.pdf; Dow Corning Form Number: 11-3716-01.

[28] Tock RW. Temperature and moisture effects on the engineering properties of silicone sealants. In: O'Connor TF, editor. Building Sealants: Materials, Properties and Performance. ASTM STP 1069. American Society for Testing and Materials; 1990, p. 167–73. doi:10.1520/STP26803S.

[29] Mullins L. Effect of stretching on the properties of rubber. Journal of Rubber Research 1947;16(12):275–89.

[30] Schmidt CM, Schoenherr WJ, Carbary LD, Takish MS. Performance properties of silicone structural adhesives. In: Parise CJ, editor. Science and Technology of Glazing Systems. American Society for Testing and Materials; 1989, p. 22–45. doi:10.1520/STP22987S.

[31] Descamps P, Hayez V, Chabih M. Next generation calculation method for structural silicone joint dimensioning. Glass Structures & Engineering 2017;2:169–82. doi:10.1007/s40940-017-0044-7.

[32] Dow Corning Corporation. Product Information: Dow Corning 993 Structural Glazing Sealant; 2011. URL: http://www.dowcorning.com/content/publishedlit/62-0918.pdf; Dow Corning Form Number: 62-0918L-01.

[33] Wang D, El-Sheikh AI. Large deflection mathematical analysis of rectangular plates. Journal of Engineering Mechanics 2005;131:809–21. doi:10.1061/(ASCE)0733-9399(2005)131:8(809).

[34] Head RN, Sechler EE. Normal Pressure Tests on Unstiffened Flat Plates; 1944. URL: https://ntrs.nasa.gov/search.jsp?R=19930086088; NACA Technical Note 943.

[35] AS 1288. Glass in Buildings – Selection and Installation; 2006. URL: http://www.standards.org.au.